ACADEMIC PRESS

Available online at www.sciencedirect.com

SCIENCE DIRECT®

Journal of Magnetic Resonance 163 (2003) 174–181

JMR Journal of Magnetic Resonance

www.elsevier.com/locate/jmr

Solution-state dynamics of sugar-connected spin probes in sucrose solution as studied by multiband (L-, X-, and W-band) electron paramagnetic resonance

Kôichi Fukui,[a,*] Tomohiro Ito,[b] Mika Tada,[a] Masaaki Aoyama,[c] Shingo Sato,[d] Jun-ichi Onodera,[d] and Hiroaki Ohya[c]

[a] *Regional Joint Research Project of Yamagata Prefecture, Yamagata Public Corporation for the Development of Industry, Matsuei 2-2-1, Yamagata 990-2473, Japan*

[b] *Graduate School of Science and Engineering, Yamagata University, Jonan 4-3-16, Yonezawa 992-8510, Japan*

[c] *Institute for Life Support Technology, Yamagata Public Corporation for the Development of Industry, Matsuei 2-2-1, Yamagata 990-2473, Japan*

[d] *Faculty of Engineering, Yamagata University, Jonan 4-3-16, Yonezawa 992-8510, Japan*

Received 29 January 2003; revised 8 May 2003

Abstract

A multiband (L-band, 0.7 GHz; X-band, 9.4 GHz; and W-band, 94 GHz) electron paramagnetic resonance (EPR) study was performed for two glycosidated spin probes, 4-(α, β-D-glucopyranosyloxy)-TEMPO (Glc-TEMPO) and 4-(α, β-D-lactopyranosyloxy)-TEMPO (Lac-TEMPO), and one non-glycosylated spin probe, 4-hydroxy-TEMPO (TEMPOL), where TEMPO = 2,2,6,6-tetramethyl-1-piperidinyloxyl, to characterize fundamental hydrodynamic properties of sugar-connected spin probes. The linewidths of these spin probes were investigated in various concentrations of sucrose solutions (0–50 wt%). The multiband approach has allowed full characterization of the linewidth parameters, providing insights into the molecular shapes of the spin probes in sucrose solution. The analysis based on the fast-motional linewidth theory has yielded anisotropy parameters of $\rho_x \approx 2.6$ and $\rho_y \approx 0.9$ for Glc-TEMPO, and $\rho_x \approx 4.2$ and $\rho_y \approx 0.9$ for Lac-TEMPO. These values indicate that the glycosidated spin probes have a prolate-type molecular shape elongated along the x-axis (NO· axis) with Lac-TEMPO elongated more remarkably, consistent with their molecular structures. The interaction parameters k (the ratios of the effective hydrodynamic volumes to the real ones) corrected for the difference in molecular shape have been estimated and found to have the relation $k(\text{TEMPOL}) < k(\text{Glc-TEMPO}) \approx k(\text{Lac-TEMPO})$. This agrees with the expectation that glycosidated spin probes can have stronger hydrogen bonding to water. Glycosidated spin probes are expected to be useful for probing sugar-involving interactions, which commonly occur in biological systems. Thus this study will provide an indispensable basis for such spin-probe studies.

Keywords: EPR; W band; L band; Linewidth; Spin probe

1. Introduction

Linewidth, as well as the g value and the hyperfine coupling constant, is one of the important parameters in electron paramagnetic resonance (EPR), containing rich information concerning the dynamics of molecules. In particular, the linewidth of nitroxyl radicals has been a subject of numerous studies, and the variation of their linewidth has been utilized to probe various parameters such as cellular cytosol viscosity [1,2], membrane fluidity [3], oxygen concentration [4], and structure of sucrose–water mixture [5,6]. Of lots of possible nitroxyl-based spin probes, sugar-connected spin probes such as 4-(D-glucopyranosyloxy)-TEMPO (Glc-TEMPO), where TEMPO = 2,2,6,6-tetramethyl-1-piperidinyloxyl, would be interesting. Valuable information concerning sugar-involving interactions in biological systems may be gained from studies using sugar-connected spin probes. In fact, Struve and McConnell [7] showed that 4-(D-galactopyranosyloxy)-TEMPO (Gal-TEMPO) can be a substrate of a transporter protein (galactoside permease)

* Corresponding author. Fax: +81-23-647-3109.
E-mail address: fukui@ckk.ymgt-techno.or.jp (K. Fukui).

1090-7807/03/$ - see front matter © 2003 Elsevier Science (USA). All rights reserved.
doi:10.1016/S1090-7807(03)00174-5

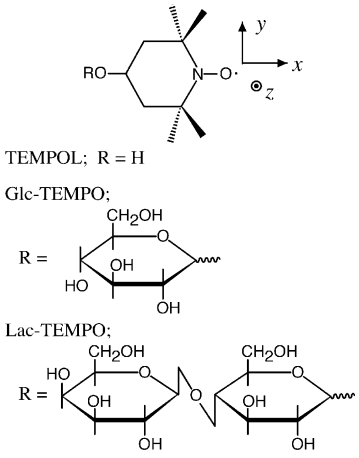

Fig. 1. Spin probes and the molecular-axis system.

and actually taken up by *Escherichia coli* cells through this protein. It is also reported that Gal-TEMPO can be a substrate of galactosidase [7,8]. Furthermore, Peerce [9] reported that Glc-TEMPO can interact with a glucose transporter, and thus may be used to probe the activities of this transporter. These possibilities have prompted us to investigate EPR linewidth properties of glycosylated spin probes to characterize their fundamental hydrodynamic properties.

In the present study, we have characterized hydrodynamic properties of two glycosidated spin probes, Glc-TEMPO and 4-(D-lactopyranosyloxy)-TEMPO (Lac-TEMPO), and one non-glycosylated spin probe, 4-hydroxy-TEMPO (TEMPOL) (Fig. 1). They were examined in various concentrations of sucrose solutions by L-band (0.7 GHz), X-band (9.4 GHz), and W-band (94 GHz) EPR spectroscopy. The multiband approach has allowed full characterization of the linewidth parameters, which permits estimation of the molecular shapes of the spin probes in solution. Sucrose solution would be a good model for cellular fluids because sucrose is often a major solute constituent in cellular fluids (particularly in plants) and bears good affinity to cells as has been demonstrated by frequent use of this disaccharide for adjustment of osmotic pressure and protection from freezing damage [10].

2. Theoretical background

In the framework of the fast-motional regime, the linewidth parameters A, B, and C can be written down in terms of the components of the rotational diffusion tensor **R**, the **g** tensor, and the hyperfine coupling tensor **A** together with an empirical parameter A^0 representing the contribution independent of the rotational diffusion. Theoretical expressions for the linewidth parameters have been given elsewhere; for example, in [11] for the case of isotropic rotational diffusion and in [12] for the case of completely anisotropic rotational diffusion. The equations for the anisotropic diffusion case can be transformed into the allowed-value equations (AVEs) with respect to the anisotropy parameters ρ_x and ρ_y ($\rho_x = R_x/R_z$ and $\rho_y = R_y/R_z$) as [12,13]

$$\alpha_{\mathrm{CB}}\rho_x = \beta_{\mathrm{CB}}\rho_y + \gamma_{\mathrm{CB}}, \tag{1.1}$$

$$\alpha_{\mathrm{AB}}\rho_x = \beta_{\mathrm{AB}}\rho_y + \gamma_{\mathrm{AB}}, \tag{1.2}$$

where the former equation comes from the division C/B and the latter from $(A - A^0)/B$. The explicit forms of α_{CB}, β_{CB}, γ_{CB}, α_{AB}, β_{AB}, and γ_{AB} have been given elsewhere [12].

The rotational diffusion tensor **R** is related to the shape and the size of the solute molecule. For an ellipsoidal solute molecule which has principal radii of r_x, r_y, and r_z, the principal components of **R** can be written as [12]

$$R_i = \frac{3k_{\mathrm{B}}T}{16\pi k\gamma_i\eta}, \quad i = x, y, z, \tag{2}$$

where k is an empirical interaction parameter accounting for non-ideal Stokes–Einstein behaviors in the solute–solvent interactions (e.g., slip), and

$$\gamma_i = \frac{r_j^2 + r_k^2}{r_j^2 Q_j + r_k^2 Q_k}, \quad i \neq j \neq k \neq i, \tag{3}$$

$$Q_i = \int_0^\infty \frac{\mathrm{d}s}{\sqrt{(r_i^2 + s)^3 (r_j^2 + s)(r_k^2 + s)}}, \tag{4}$$

and the other symbols have usual meanings. The rotational correlation time τ_{R} is also used to characterize the molecular tumbling motion, and conventionally defined as

$$\tau_{\mathrm{R}}^{-1} = 2R_z\sqrt{(\rho_s - \delta)(\rho_s + 2\delta)}, \tag{5}$$

where

$$\rho_{\mathrm{s}} = 1 + \rho_x + \rho_y, \tag{6}$$

$$\delta = \pm\sqrt{\frac{(1-\rho_x)^2 + (1-\rho_y)^2 + (\rho_x - \rho_y)^2}{2}}. \tag{7}$$

The sign of δ should be positive when the molecular ellipsoid is prolate or can be approximated as prolate, and negative when the ellipsoid is oblate or can be approximated as oblate [12]. Using Eq. (2) and the equation for the volume of the ellipsoid, $V = 4\pi r_x r_y r_z/3$, one can rewrite Eq. (5) as

$$\tau_{\mathrm{R}} = \frac{k f_{\mathrm{shape}}\eta V}{k_{\mathrm{B}}T}, \tag{8}$$

where

$$f_{\mathrm{shape}} = \frac{2\gamma_z}{r_x r_y r_z\sqrt{(\rho_{\mathrm{s}} - \delta)(\rho_{\mathrm{s}} + 2\delta)}}. \tag{9}$$

We may call f_{shape} a shape-correction factor. Corrected by f_{shape}, the k values based on Eq. (8) can be compared with one another regardless of a difference in molecular shape. When the molecule has a uniaxial symmetry, Eq. (4) can be reduced to an analytical form, and thus ρ_x (or ρ_y) and f_{shape} can be expressed analytically in terms of the ratio of the principal radii r_x/r_z (or r_y/r_z) [14,15].

3. Experimental

3.1. Material

Glc-TEMPO was prepared by deacetylation of tetra-O-acetylated Glc-TEMPO [16] using sodium methoxide according to a standard method. Lac-TEMPO was synthesized in an analogous manner. The glycosidated spin probes used in this study were mixtures of the α- and β-anomers. For Glc-TEMPO, the ratio was determined as $\alpha{:}\beta \approx 1{:}3$ [16]. Although the β-anomer of Glc-TEMPO was purified and examined by X-band EPR spectroscopy, no differences were found between the EPR results of the purified β-anomer and the mixture. Hence, no further attempts were made to purify the anomers.

3.2. Measurements

X-band EPR spectra were recorded on a JEOL RE-3X spectrometer. W-band EPR spectra were obtained on the spectrometer constructed in our laboratory. Instrumental details were described previously [17]. Briefly, the spectrometer consists of a wide-bore superconducting magnet (Suzuki Shokan; bore diameter = 100 mm), a cavity-stabilized Gunn oscillator (Keycom, CSO-01), dielectric waveguides (Keycom, DW110A), a Fabry-Pérot cavity (fabricated in Keycom), a balanced mixer (MRI, BMR1W), and a lock-in amplifier (NF electronic Instruments, 5610B). Tuning of the Fabry–Pérot cavity was made by adjusting the position of one side of the mirrors with a stepping motor (Suruga Seiki). This mirror also serves as a sample stage, on which ~1 μl of sample solution was dropped and covered with a coverglass. L-band EPR measurements were carried out on a home-built spectrometer [18]. A sample solution (500 μl) in a conical tube was measured using a surface-coli resonator. For all measurements, temperature was constantly monitored with a digital thermometer (Testo, GT-110). No particular degas treatments were performed because the spin probes investigated here have relatively large unresolved hyperfine splittings and thus broadening due to dioxygen is negligible. Experimental conditions are as follows: For L band: microwave frequency, 0.723–0.725 GHz; microwave power, 10 mW; modulation width, 0.05 mT; temperature, ~25 °C; samples, 0.5 mM × 500 μl. For X band: microwave frequency, ~9.44 GHz; microwave power, 5 mW; modulation width, 0.05 mT; temperature, ~25 °C; samples, 0.1 mM × 10 μl. For W band: milliwave frequency, ~94.0 GHz; milliwave power, 5 mW; modulation width, 0.13 mT (TEMPOL), 0.25 mT (Glc-TEMPO and Lac-TEMPO); temperature, 10–15 °C; samples, 1 mM × 1 μl. The linewidths of the spin probes at W band were found to be much larger than those at X band and L band, so that larger field modulation was applied in W-band experiments.

3.3. Analysis

The linewidth parameters were determined by numerical fitting of EPR spectra. The fitting function employed was a sum of three lineshape functions, each of which corresponds to one hyperfine line due the ^{14}N nucleus;

$$F(B_0) = a\sum_{M_I} f(B_0 - B_{\text{res}}(M_I), W_{\text{pp}}(M_I)) + b, \tag{10}$$

where a and b adjust the overall signal height and the baseline offset, respectively. The symbols $B_{\text{res}}(M_I)$ and $W_{\text{pp}}(M_I)$ denote the position and the peak-to-peak linewidth of the $I_z(^{14}\text{N}) = M_I$ hyperfine line, respectively. The peak-to-peak linewidth is written as

$$W_{\text{pp}}(M_I) = A_{\text{pp}} + B_{\text{pp}}M_I + C_{\text{pp}}M_I^2, \tag{12}$$

where we have added the suffix "pp" to indicate that they are derived from the peak-to-peak linewidths. (An additional suffix may be used to distinguish the bands of the EPR experiments as B_{pp}^{Λ}; Λ = L, X, and W). The lineshape function $f(\Delta B, W_{\text{pp}})$ was assumed to be a weighted sum of the Gaussian and Lorentzian functions as

$$f(\Delta B, W_{\text{pp}}) = c_{\text{L}}\text{Lorentzian}(\Delta B, W_{\text{pp}}) + (1 - c_{\text{L}})\text{Gaussian}(\Delta B, W_{\text{pp}}). \tag{13}$$

The Lorentzian and Gaussian functions are set to have the same peak-to-peak linewidth, and normalized to give unity when doubly integrated from $-\infty$ to ∞. The four parameters A_{pp}, B_{pp}, C_{pp}, and c_{L} were varied to achieve the best fits to experimental spectra (with additional variations of $B_{\text{res}}(M_I)$'s for adjustment of the line positions). For the W-band spectrum of Lac-TEMPO in 22.6 wt% sucrose solution, however, the fitting resulted in unexpected negative C_{pp}, though its magnitude was small. Thus we fixed C_{pp} at zero only for this case.

For the principal components of the **g** and **A**(^{14}N) tensors, literature values for TEMPOL were used; g_x, g_y, g_z = 2.0085, 2.0059, and 2.0021 and A_x, A_y, and A_z = 0.77, 0.70, 3.62 mT [11], where the axis system is shown in Fig. 1. The η/T-independent term A_{pp}^0 was determined from the intercept in the A_{pp}–B_{pp} plot of the W-band data: resulting values are $A_{\text{pp}}^0 = 0.149 \pm 0.003$ mT for TEMPOL, 0.125 ± 0.004 mT for Glc-TEMPO, and

0.132 ± 0.021 mT for Lac-TEMPO. Anisotropy parameters ρ_x and ρ_y, which were assumed to be independent of η/T, were determined using the AVEs (Eqs. (1.1) and (1.2)), where the $(A_{pp} - A^0_{pp})/B_{pp}$ and C_{pp}/B_{pp} values were determined from the W-band data and X-band data, respectively. Rotational correlation times were obtained on the basis of Eq. (5), where R_z was determined by searching the value that minimizes

$$[(B_{pp} - B^{cal}_{pp})^2 + (C_{pp} - C^{cal}_{pp})^2]^{1/2}$$

for each set of the X-band data (B_{pp}, C_{pp}). Here B^{cal}_{pp} and C^{cal}_{pp} were calculated using [12, Eq. (2)].

The viscosities of sucrose solutions were calculated from the handbook values by interpolation [19]. Solvent-excluded volumes of spin probes were obtained using Cambridge soft corporation CS Chem 3D.

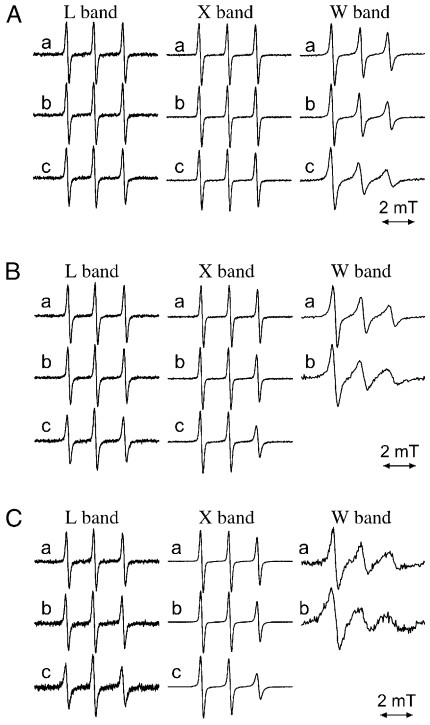

Fig. 2. L-, X-, and W-band EPR spectra of TEMPOL (A), Glc-TEMPO (B), and Lac-TEMPO (C) in various sucrose solutions (a, 0 wt%; b, 22.6 wt%; and c, 41.6 wt%). For L band: $\nu = 0.723$–0.725 GHz, $T = 25$ °C; X band: $\nu = 9.44$ GHz; $T = 25$ °C; and W band: $\nu = 94.0$ GHz; $T = 10$–15 °C.

4. Results

4.1. Linewidth parameters

Representative multiband EPR spectra of TEMPOL, Glc-TEMPO, and Lac-TEMPO are shown in Fig. 2, and resulting linewidth parameters are plotted in Fig. 3. The present results are in line with theoretical and experimental results in literature [11,20]: Firstly, the η/T dependence became remarkable with the increase of the molecular size as TEMPOL < Glc-TEMPO < Lac-TEMPO, which is consistent with the Stokes–Einstein model. Secondly, while A_{pp} showed very little variation in the L- and X-band data, A_{pp} in the W-band data exhibited notable η/T dependence. This is because the η/T-dependent contribution exceeds the η/T-independent one A^0_{pp} at W band. (As a result of the combination

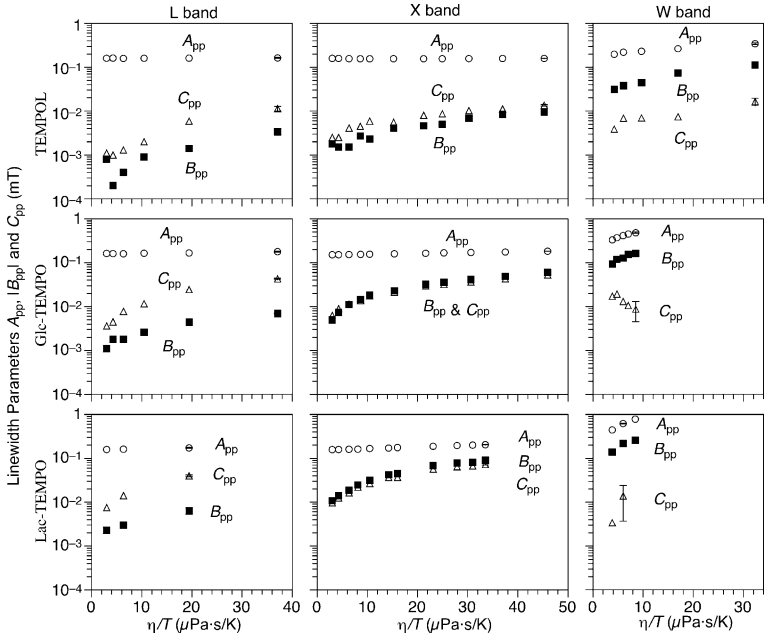

Fig. 3. η/T dependence of the linewidth parameters, A_{pp} (○), B_{pp} (■), and C_{pp} (△). Bars denote standard deviations ($n = 3$ for W- and X-band data and $n = 2$ for L-band data) for representative data points.

of the above two trends, we could not obtain enough clear signals from Glc-TEMPO and Lac-TEMPO in sucrose solutions of 30 wt% and above.) Thirdly, B_{pp} increased almost linearly with the increase of the EPR frequency. This is in agreement with the theoretical expectation that B_{pp} is essentially (or exactly when the non-secular effects are negligible) proportional to the resonance field. Lastly, C_{pp} did not increase with the increase of the EPR frequency. This also agrees well with the theoretical expectation that C_{pp} is essentially independent of the EPR frequency. This nature makes C_{pp} relatively unimportant at W band (less than ~10% of B_{pp}). As a result of this, the C_{pp} values obtained for Glc-TEMPO and Lac-TEMPO at W band are unfortunately not very reliable.

4.2. Lorentzian ratio

The fitting of the EPR spectra also allowed us to determine η/T dependence of the Lorentzian ratio. Since the η/T-independent term A^0_{pp} comes mostly from the inhomogeneously broadened unresolved ^{1}H hyperfine splittings, the lineshape should be Gaussian when $A_{pp} \approx A^0_{pp}$. On the other hand, the lineshape should approach Lorentzian as A_{pp} increases owing to a decrease of the rotational diffusion rate. Resulting Lorentzian ratios showed that this is indeed the case: the lineshape for TEMPOL was invariably relatively close to Gaussian at X and L bands ($c_L \sim 0.3$–0.5). Under the same conditions, the lineshapes for Glc-TEMPO and Lac-TEMPO varied from a mixture of Gaussian and Lorentzian at low η/T ($c_L \sim 0.4$–0.5) to the one close to Lorentzian at high η/T ($c_L \sim 0.7$–0.8). At W band, on the other hand, the lineshape of the three spin probes was invariably close to Lorentzian ($c_L \sim 0.7$–1.0).

4.3. Anisotropy parameters

In order to test the relevance of the anisotropy in the rotational diffusion, we first determined the rotational correlation times by assuming isotropic rotational diffusion. Results are plotted against η/T in Fig. 4, where $\tau_R(A)$, $\tau_R(B)$, and $\tau_R(C)$ are correlation times resulting individually from the linewidth parameters A_{pp}, B_{pp}, and C_{pp}, respectively. The three types of correlation times should coincide with one another when the rotational diffusion is actually isotropic. Indeed the differences between $\tau_R(A)$, $\tau_R(B)$, and $\tau_R(C)$ for TEMPOL are not significant when compared with the error ranges. Thus we conclude that the anisotropy in the rotational diffusion is not important for TEMPOL. For Glc-TEMPO and Lac-TEMPO, on the other hand, the differences between $\tau_R(A)$, $\tau_R(B)$, and $\tau_R(C)$ are significantly large. Interestingly, $\tau_R(A)$, $\tau_R(B)$, and $\tau_R(C)$, respectively, form well-defined curves in an EPR-frequency independent manner, which strongly suggests that the anisotropy in the rotational diffusion is not negligible for Glc-TEMPO and Lac-TEMPO.

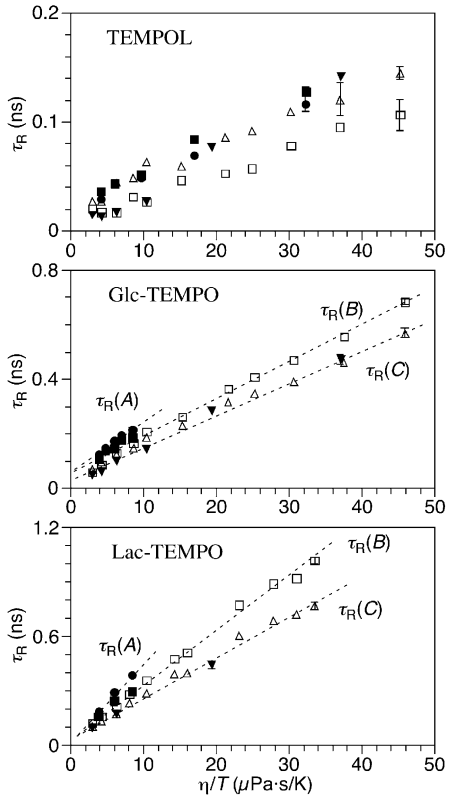

Fig. 4. η/T dependence of the rotational correlation times obtained under the assumption of isotropic rotational diffusion. Plotted are $\tau_R(A)$ values from W-band data (●), $\tau_R(B)$ values from W-band data (■), and X-band data (□), $\tau_R(C)$ values from X-band data (△) and L-band data (▼). Dashed lines are drawn to guide the eyes. Bars denote standard deviations.

The above results indicate that further analysis taking into consideration the anisotropy of the rotational diffusion is desirable for Glc-TEMPO and Lac-TEMPO. Following Kowert [13] and Budil et al. [12], we determined the anisotropy parameters ρ_x and ρ_y on the basis of the AVEs (Eqs. (1.1) and (1.2)). The two AVEs give a set of two lines, and their intercept indicates the ρ_x and ρ_y values. Resulting lines for Glc-TEMPO and Lac-TEMPO are shown in Fig. 5 along with those for the

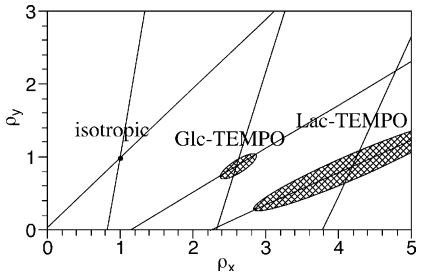

Fig. 5. Determinations of the anisotropy parameters ρ_x and ρ_y. Hatched ellipses denote estimated error ranges. Lines corresponding to the isotropic case are also shown for comparison.

Table 1
Important parameters for TEMPOL, Glc-TEMPO, and Lac-TEMPO

	TEMPOL	Glc-TEMPO	Lac-TEMPO
A^0_{pp} (mT)	0.149 ± 0.003	0.125 ± 0.004	0.132 ± 0.021
$(A^W_{pp} - A^0_{pp})/\lvert B^W_{pp}\rvert$		2.19 ± 0.03	2.33 ± 0.10
$C^X_{pp}/\lvert B^X_{pp}\rvert$		0.895 ± 0.009	0.819 ± 0.007
ρ_x	1[a]	2.6	4.2
ρ_y	1[a]	0.9	0.9
r_x/r_z[b]	1[a]	2.6	3.7
f_{shape}[b]	1[a]	1.23	1.49
V (Å^3)[c]	180	330	470

[a] Fixed value.
[b] Obtained under the assumption $r_y = r_z$.
[c] Obtained by molecular model calculation.

isotropic case. The ratios of the linewidth parameters used for the calculations of the lines are listed in Table 1. These ratios are significantly different from those expected for the isotropic case $(A^W_{pp} - A^0_{pp})/B^W_{pp} = -1.913$ and $C^X_{pp}/B^X_{pp} = -1.062$. In harmony with this, the intersections are significantly different from that for the isotropic case $\rho_x = \rho_y = 1$, appearing at $\rho_x \approx 2.6$ and $\rho_y \approx 0.9$ for Glc-TEMPO and $\rho_x \approx 4.2$ and $\rho_y \approx 0.9$ for Lac-TEMPO. Estimated error ranges are illustrated as ellipses in Fig. 5. The error range for Lac-TEMPO is unfortunately very large because of the large uncertainty in $(A^W_{pp} - A^0_{pp})/B^W_{pp}$ for this spin probe. Nevertheless, the trend, $1 < \rho_x$(Glc-TEMPO) $< \rho_x$(Lac-TEMPO), is outstanding even under such a large uncertainty.

4.4. Rotational correlation time and interaction parameter

Fig. 6 shows the η/T dependence of the rotational correlation time τ_R obtained from the X-band linewidth parameters using the above determined ρ_x and ρ_y values ($\rho_x = \rho_y = 1$ is assumed for TEMPOL). To determine the interaction parameter corrected for the difference in the molecular shape, we must calculate the shape-correction factor f_{shape} (Eq. (9)). In the calculation, we approximated the rotational diffusion tensors as uniaxial

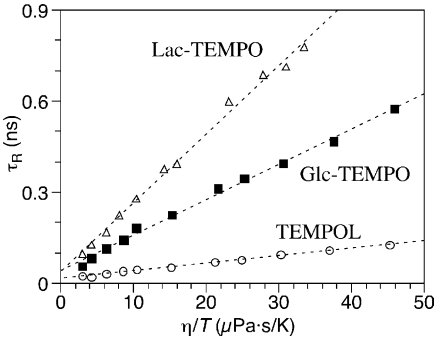

Fig. 6. η/T dependence of the rotational correlation time τ_R obtained with the anisotropy in the rotational diffusion taken into consideration for TEMPOL (○), Glc-TEMPO (■), and Lac-TEMPO (△). Dashed lines represent simple linear fittings of the data.

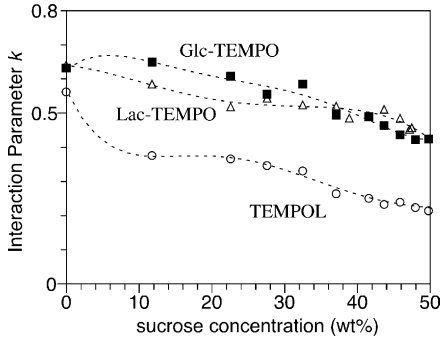

Fig. 7. Sucrose concentration dependence of the interaction parameter k for TEMPOL (○), Glc-TEMPO (■), and Lac-TEMPO (△). Dashed lines are eye guides generated by data fitting to the fifth-order polynominal.

(i.e., $\rho_y = 1$) because the resulting ρ_y values are actually close to unity and because this approximation allows analytical calculation of Eq. (4) [14,15]. Then, by using the relation $\rho_x = \gamma_z/\gamma_x$ and Eqs. (3) and (4), we obtained $r_x/r_z \approx 2.6$ for Glc-TEMPO and $r_x/r_z \approx 3.7$ for Lac-TEMPO, which provide $f_{shape} = 1.23$ for Glc-TEMPO and 1.49 for Lac-TEMPO. For TEMPOL, which is assumed to be spherical, $f_{shape} = 1$ was obtained. Additionally, molecular volumes (solvent-excluded volumes) were estimated by molecular model calculation as $V = 180$ Å^3 for TEMPOL, 330 Å^3 for Glc-TEMPO, and 470 Å^3 for Lac-TEMPO. With these values, we obtained the shape-corrected interaction parameters k, which are plotted against sucrose concentrations in Fig. 7.

5. Discussion

We have analyzed the multiband EPR data in the framework of the fast-motional regime [21], and obtained several parameters relevant to the hydrodynamic properties of the spin probes. The anisotropy parameters ρ_x and ρ_y are related to the shape of the molecule: roughly speaking, $\rho_i > 1$ means that the molecular ellipsoid is elongated along the i axis compared to the z axis ($r_i > r_z$), and $\rho_i < 1$ means the opposite. Thus the

resulting ρ_x and ρ_y values indicate that the molecules of Glc-TEMPO and Lac-TEMPO are approximately in a prolate shape elongated along the x axis. For nitroxyl radicals, the molecular x axis is along the N–O· direction (Fig. 1). Thus the obtained relations, $\rho_x > 1$ and $\rho_y \approx 1$, are totally consistent with their molecular structures, where the glucosyl and lactosyl groups are connected at the *para* position of NO·. Furthermore, the result that the ρ_x value for Lac-TEMPO is larger than that for Glc-TEMPO agrees with the fact that the lactosyl group is larger than the glucosyl group. The ratios of the principal radii of the molecular ellipsoids have been estimated as $r_x/r_z \approx 2.6$ for Glc-TEMPO and $r_x/r_z \approx 3.7$ for Lac-TEMPO. According to molecular models, TEMPOL, the glucosyl group and the galactosyl group are roughly in the same size; i.e., a sphere of $\sim$3.5 Å radius. Thus, if the constituting groups are aligned linearly, Glc-TEMPO would have $r_x/r_z \approx 2$ and Lac-TEMPO would have $r_x/r_z \approx 3$. Such a molecular geometry can be supported by the previous X-ray crystallographic result for tetra-O-acetylated Glc-TEMPO [22]. The r_x/r_z values based on the molecular models are comparable with those estimated from the anisotropy parameters. Although quantitative agreements are not excellent, the agreements are still satisfactory in consideration of the large uncertainties in ρ_x and ρ_y.

Anisotropy parameters of some other spin probes and spin adducts have been reported in literature. For example, Budil et al. [12] obtained $\rho_x \approx 1.8$ and $\rho_y \approx 1.5$ for TEMPONE-d^{16} in toluene-d^8. They pointed out that these values agree with those expected from a molecular model ($\rho_x = 1.35$ and $\rho_y = 0.97$). These values are fairly close to the isotropic case ($\rho_x = \rho_y = 1$). This is consistent with our results showing $\rho_x \approx \rho_y \approx 1$ for TEMPOL, whose molecular dimensions are similar to those of TEMPONE. Smirnova et al. [23] investigated tetradecyl and methyl adducts of phenyl *tert*-butylnitrone (PBN), and estimated as $\rho_x \approx \rho_y \approx 1.0$, and $\rho_x \approx 2.7$ and $\rho_y \approx 3.6$, respectively. They attributed the nearly isotropic ρ_x and ρ_y values for tetradecyl-PBN to a folding of the long alkyl chain. The anisotropy parameters for the latter adduct indicate an oblate-type molecular shape, which is consistent with its molecular structure. A more complex spin probe, 3-doxyl-17β-hydroxy-5α-androstane (referred to as Probe #1 as in the original paper), was also investigated, and $\rho_x \approx 1.6$ and $\rho_y \approx 5.8$ were reported [24]. Quite interestingly, the relation $\rho_x > \rho_y \approx 1$ for Glc-TEMPO and Lac-TEMPO is reversed in Probe #1. For Probe #1,the long axis is expected to be perpendicular to the N–O· direction within the C–N(–O·)–C plane. Hence the reverse of the relation well reflects the difference in molecular shape between the two types of spin probes, reinforcing the validity of the anisotropy parameters.

The interaction parameter k is a measure of deviation from the ideal Stokes–Einstein behavior in the solute–solvent interactions. A decrease of k from unity indicates that the solute-solvent interactions are weaker than those expected for the ideal case [25]. Such a decrease usually occurs owing to the slip between the solute and solvent molecules (or between the solvent molecules in one sphere and the next sphere). Fig. 7 shows that the interaction parameters of Glc-TEMPO and Lac-TEMPO are invariably larger than that of TEMPOL. This is quite reasonable because the glycosidated spin probes can have stronger hydrogen bonding to water molecules, which will make the slip of the solvent less frequent. The decrease of k with the increase of sucrose concentration is also reasonable because the increase of sucrose would decrease the number of water molecules that can interact with the spin probes. Hydrodynamic properties of non-glycosidated spin probes in sucrose solution have been investigated by Roozen and Hemminga [5,6]. They found that the interaction parameter k decreases abruptly when the sucrose concentration exceeds $\sim$40 wt%. This abrupt decrease was attributed to some solution structural change in the sucrose–water mixture. It was reported that all the water molecules become to be involved in hydrogen bonding to sucrose (directly or indirectly) around the concentration of 30–40 wt%, which leaves very few water molecules that can form hydrogen bonding to the non-glycosylated spin probes [5,6]. Fig. 7 indeed exhibits a turning point around the sucrose concentration of 30–40 wt% for TEMPOL, which appears to be consistent with the findings by Roozen and Hemminga [5,6]. Furthermore, similar turning points can be seen around 40 wt% in the plots for Glc-TEMPO and Lac-TEMPO, though they are less clear. These results suggest that the change in the sucrose-solution structure affects less the hydrodynamic properties of the glycosidated spin probes. This is not surprising because the sugar group in the glycosylated spin probes is likely to retain some degree of hydrogen bonding to water in such high concentrations of sucrose solutions.

References

[1] A.D. Keith, W. Snipes, Science 183 (1974) 666–668.
[2] B. Schobert, D. Marsh, Biochim. Biophys. Acta 720 (1982) 87–95.
[3] L. Calucci, F. Navari-Izzo, C. Pinzino, C.L.M. Sgherri, J. Phys. Chem. B 105 (2001) 3127–3134.
[4] H.M. Swartz, J.F. Glockner, Measurements of the concentration of oxygen in biological systems using EPR techniques, in: A.J. Hoff (Ed.), Advanced EPR: Applications in Biology and Biochemistry, Elsevier, Amsterdam, 1989, pp. 753–784.
[5] M.J.G.W. Roozen, M.A. Hemminga, J. Phys. Chem. 94 (1990) 7326–7329.
[6] M.A. Hemminga, I.J. van den Dries, Spin label applications to food science, in: L.J. Berliner (Ed.), Biological Magnetic Resonance, vol. 14, Plenum, New York, 1998, pp. 339–366.

[7] W.G. Struve, H.M. McConnell, Biochem. Biophys. Res. Commun. 49 (1972) 1631–1637.
[8] N.R. Plessas, I.J. Goldstein, Carbohydr. Res. 89 (1981) 211–220.
[9] B.E. Peerce, Biochemistry 30 (1991) 4186–4192.
[10] K.T. Tokuyasu, J. Cell Biol. 57 (1973) 551–565.
[11] N.M. Atherton, Principles of Electron Spin Resonance, Ellis Horwood, New York, 1993.
[12] D.E. Budil, K.A. Earle, J.H. Freed, J. Phys. Chem. 97 (1993) 1294–1303.
[13] B.A. Kowert, J. Phys. Chem. 85 (1981) 229–235.
[14] J.S. Hwang, R.P. Mason, L.-P. Hwang, J.H. Freed, J. Phys. Chem. 79 (1975) 489–511.
[15] D. Hoel, D. Kivelson, J. Chem. Phys. 62 (1975) 1323–1326.
[16] S. Sato, T. Kumazawa, S. Matsuba, J. Onodera, M. Aoyama, H. Obara, H. Kamada, Carbohydr. Res. 334 (2001) 215–222.
[17] K. Fukui, T. Ito, H. Ohya, High-frequency (W-band) EPR studies of biological samples, in: A. Kawamori, J. Yamauchi, H. Ohta (Eds.), EPR in the 21st Century: Basics and Applications to Material, Life and Earth Sciences, Elsevier, Amsterdam, 2002, pp. 818–823.
[18] K. Oikawa, T. Ogata, Y. Lin, T. Sato, R. Kudo, H. Kamada, Anal. Sci. 11 (1995) 885–888.
[19] (a) Kagaku-binran Kiso-hen vol. II (Japanese), p. 48, Maruzen, Tokyo, 1993;
(b) M. Mathlouthi, J. Genotelle, Rheological properties of sucrose solutions and suspensions, in: M. Mathlouthi, P. Reiser (Eds.), Sucrose: Properties and Applications, Aspen Publishers, New York, 1994, pp. 126–154.
[20] A.I. Smirnov, R.L. Belford, R.B. Clarkson, Comparative spin label spectra at X-band and W-band, in: L.J. Berliner (Ed.), Biological Magnetic Resonance, vol. 14, Plenum, New York, 1998, pp. 83–107.
[21] Additional calculations using a general simulation program (NLSL) were made to check the validity of the fast-motional approach to such severely distorted spectra as those observed for Lac-TEMPO at W band. The program NLSL is based on general formulae and valid for both the fast-motional and slow-motional cases [D.E. Budil, S. Lee, S. Saxena, J.H. Freed, J. Mag. Res on. A 120 (1996) 155–189], Comparison between the spectra produced by this general program and those obtained solely on the basis of the fast-motional theory showed that these two types of simulated spectra coincide with each other even when $\tau_R \approx 0.23$ ns and $B_{res} \approx 3350$ mT. This indicates that the fast-motional approach is still valid for the W-band spectrum of Lac-TEMPO in 22.6 wt% sucrose ($\tau_R \approx 0.23$ ns).
[22] F. Cinget, D. Gagnaire, A. Grand, P.J.A. Vottero, Carbohydr. Res. 218 (1991) 1–8.
[23] T.I. Smirnova, A.I. Smirnov, R.B. Clarkson, R.L. Belford, Y. Kotake, E.G. Janzen, J. Phys. Chem. B 101 (1997) 3877–3885.
[24] T.I. Smirnova, A.I. Smirnov, R.B. Clarkson, R.L. Belford, J. Phys. Chem. 99 (1995) 9008–9016.
[25] S.A. Zagar, J.H. Freed, J. Chem. Phys. 77 (1982) 3344–3359.